Functional regression for space-time prediction of precipitation-induced shallow landslides in South Tyrol, Italy

Mateo Moreno[1*], Luigi Lombardo[1], Stefan Steger[2], Lotte de Vugt[3], Thomas Zieher[4], Alice Crespi[5], Francesco Marra[6], Cees van Westen[1], Thomas Opitz[7]

Abstract

Shallow landslides are geomorphic hazards in mountainous terrains across the globe. Their occurrence can be attributed to the interplay of static and dynamic landslide controls. In previous studies, data-driven approaches have been employed to model shallow landslides on a regional scale, focusing on analyzing the spatial aspects and time-varying conditions separately. Still, the joint assessment of shallow landslides in space and time using data-driven methods remains challenging. This study aims to predict the occurrence of precipitation-induced shallow landslides in space and time within the Italian province of South Tyrol (7,400 km^2). In this context, we investigate the benefits of considering precipitation leading to landslide events as a functional predictor, in contrast to conventional approaches that treat precipitation as a scalar predictor. We built upon hourly precipitation analysis data and past landslide occurrences from 2012 to 2021. We implemented a novel functional generalized additive model to establish statistical relationships between the spatiotemporal occurrence of shallow landslides, various static factors included as scalar predictors, and the hourly precipitation pattern preceding a potential landslide used as a functional predictor. We evaluated the resulting predictions through several cross-validation routines, achieving high model performance scores. To showcase the model capabilities, we performed a hindcast for the storm event in the Passeier Valley on August 4th and 5th, 2016. This novel approach enables the prediction of landslides in space and time for large areas by accounting for static and dynamic functional landslide controls, seasonal effects, statistical uncertainty, and underlying data limitations.

Key points

- We integrated static scalar and dynamic functional controls to predict shallow landslides in space and time.
- The functional regression framework accounts for errors in the landslide data, has a high performance, and keeps model interpretability.
- Our approach can be potentially used for hindcasting, nowcasting, and predicting landslide occurrence under what-if precipitation scenarios.

Plain language summary

Shallow landslides are natural hazards in mountain regions, often triggered by intense and prolonged precipitation. Predicting where and when landslides may occur is crucial as it is the foundation for early warning systems and can help reduce their impacts on society and the environment. This study tested an approach to predict precipitation-induced landslides across space and time in South Tyrol, Italy. Our approach uses hourly precipitation data and records of past landslides to predict landslide occurrence. Unlike traditional approaches, ours integrates static (e.g., lithology, land cover, topography) and dynamic factors and leverages the entire precipitation time series as a functional predictor in the modeling framework. Our model also accounts for seasonal effects and errors inherent in the landslide data. It had a relatively high performance score and was tested to hindcast the landslides triggered during the storm event in the Passeier Valley on August 4th and 5th, 2016.

Keywords: Space-time modeling; FGAMs; Functional predictors; Precipitation time series; INCA

---

[1]Faculty of Geo-Information Science and Earth Observation (ITC), University of Twente, Enschede, Netherlands
[2]GeoSphere Austria, Vienna, Austria
[3]Department of Geography, University of Innsbruck, Innsbruck, Austria
[4]Austrian Research Centre for Forests (BFW), Innsbruck, Austria
[5]Center for Climate Change and Transformation, Eurac Research, Bolzano, Italy
[6]Department of Geosciences, University of Padova, Padova, Italy
[7]Biostatistics and Spatial Processes, INRAE, Avignon, France

1. Introduction

Landslides are ubiquitous geomorphic hazards in mountainous regions across the globe, resulting in substantial annual economic, societal, and environmental consequences along with fatalities (Froude & Petley, 2018; Kirschbaum et al., 2015; Nadim et al., 2006). Climate change and environmental shifts point to growing landslide hazards of particularly fast-moving, rainfall-induced landslides (Gariano & Guzzetti, 2016; IPCC, 2022; Jakob, 2022; Maraun et al., 2022; Ozturk et al., 2022). Reliable landslide predictions are foundational for landslide early warning systems (LEWS) and can help reduce the impacts of landslides. Thus, ensuring reliable predictions of landslides and their resultant impacts is paramount. Nevertheless, the success of such predictions is intrinsically linked to the comprehensive understanding of the underlying factors driving slope instability (Glade et al., 2012).

The causes of landslides arise from a complex interplay between predisposing, preparatory, and triggering environmental factors. Predisposing factors, such as topography and material properties, represent static ground conditions that render a location more or less susceptible to landsliding. On the other hand, preparatory and triggering factors, such as precipitation and snowmelt, reflect the dynamic conditions that may either substantially influence the stability of a slope or directly initiate the slope movement (Crozier, 1986; Glade et al., 2012). Therefore, adequate integration of the static and dynamic controls is critical to achieving reliable landslide assessments (Corominas et al., 2014; Westen et al., 2006).

Assessing landslides inherently depends on the scale of the analysis, the purpose, and data availability and quality (Aleotti & Chowdhury, 1999; Fell et al., 2008; Glade et al., 2012; Guzzetti et al., 2005; Westen et al., 2008). For regional-scale assessments, data-driven models are widely used to evaluate both the spatial aspect –determining 'where' landslides may likely occur– and the temporal one –determining 'when' landslides may likely occur. Data-driven landslide susceptibility models address the spatial component by deriving statistical relationships between past landslide occurrences and a set of static environmental factors, enabling the estimation of the spatial propensity of an area to experience slope instabilities (Alvioli et al., 2024; Bryce et al., 2024; Elia et al., 2023; Goetz et al., 2015; Opitz et al., 2022; Tanyas et al., 2019). The resulting maps are frequently used and considered relevant in land use and spatial planning. Limitations in the applicability of these models arise, given that the landslide inventories rarely provide complete representations of past landslides, and strategies to account for them are rarely implemented (Bornaetxea et al., 2018; Knevels et al., 2020; Lima et al., 2021; Steger et al., 2021).

The temporal component is linked to the assessment of the dynamic triggering factors. In our case, Italy, precipitation is identified as the primary factor influencing the timing of shallow landslide occurrence (Brunetti et al., 2010). In this context, data-driven approaches are applied to elaborate on critical triggering conditions, with empirical precipitation or rainfall thresholds commonly used to predict landslide occurrence (Gariano et al., 2015; Niyokwiringirwa et al., 2024; Peruccacci et al., 2017; Segoni et al., 2018). These thresholds are derived by linking past landslide occurrence data with associated precipitation measures (e.g., rainfall intensity and duration, cumulative storm or event rainfall and duration) and serve as foundations for early warnings (Gariano et al., 2015; Guzzetti et al., 2020). These methods frequently focused on the triggering precipitation conditions, and comparatively few studies address the effects of preparatory factors and hydrological effects (Bogaard & Greco, 2016; Greco et al., 2023; Monsieurs et al., 2019; Steger et al., 2023).

The joint assessment of spatial and temporal aspects in landslide modeling is seldomly addressed in the literature, though recent studies highlight its promising potential (Ahmed et al., 2023; Bajni et al., 2023; Caleca et al., 2024; Knevels et al., 2020; Moreno et al., 2024; Steger et al., 2024). These approaches integrate static and dynamic landslide controls as scalar values, such as precipitation (Wang et al., 2022), soil moisture (Stanley et al., 2021), ground motion (Dahal, Tanyas, et al., 2024), temperature (Loche et al., 2022), and snowmelt (Camera et al., 2021), by dissecting the temporal component and aggregating dynamic predictors over time (e.g., years, seasons, months, days, or hours). For instance, in Wang et al. (2022), landslide probabilities were estimated over a 31-year period by clustering the landslide inventory according to the designated year of occurrence and analyzing different rainfall metrics for each year. Similarly, in Dahal et al. (2024), the authors developed seasonal landslide predictive models by incorporating various rainfall and ground motion metrics, using the landslide inventories mapped due to the Gorkha earthquake in 2015 and the pre-monsoon and post-monsoon seasons in the subsequent years. In Steger et al. (2024), a dynamic shallow landslide model was devised by integrating static ground conditions with cumulative daily precipitation, expressed as medium-term preparatory and short-term triggering precipitation. Lombardo et al. (2020) developed a Bayesian model for space-time trends in a century-spanning observation dataset for the Collazzone area, Italy, by combining static predictors with random effects representing unobserved environmental triggers, such as extreme precipitation events. In Knevels et al. (2020), by combining data from weather stations and ground-based radar, 3-hour rainfall intensity and 5-day antecedent rainfall were used along with static factors to assess the landslide triggered after a particular storm event.

A relevant issue arises when using scalar values to aggregate dynamic properties over time, as this approach overlooks the potential insights a data-driven model could derive from information on the entire time series. To date, relatively few studies have focused on integrating static and dynamic factors while leveraging the functional nature of dynamic predictors, with most prioritizing performance over interpretability. For example, in Fang et al. (2023), a deep learning architecture initially designed for speech recognition was applied to incorporate daily rainfall time series in a landslide predictive model. This resulted in a substantial improvement in predictive power of ~20% compared to models that rely on scalar rainfall representations. Lim et al. (2024) extended the findings on Fang et al. (2023) by testing a different deep learning architecture in a data-scarce environment using daily rainfall, reporting similar enhanced performances. In another study, Dahal et al. (2024) considered ground motion as a functional predictor alongside static controls to predict landslide occurrence, achieving an improvement of 16% in the predictive capabilities compared to a model using only scalar inputs.

This study focuses on space-time shallow landslide modeling. We build upon previous work (Moreno et al., 2024; Steger et al., 2024), intending to test the benefits of accounting for hourly precipitation leading to landslide occurrence as a functional predictor. We account for errors in the available landslide data, provide interpretable results, and demonstrate the practical application by hindcasting the landslides triggered by a storm event in the study area. We perform the analysis in the Italian province of South Tyrol, covering a 10-year period (2012-2021). Specifically, we use functional regression to integrate hourly precipitation time series, static ground conditions, and seasonal effects while accounting for data limitations.

In the remainder of the paper, Section 2 outlines the study area, the landslide data, and the environmental predictors we use in our analysis. Then, Section 3 provides the necessary background on the functional regression framework along with the data sampling strategy, feature extraction, and model validation approaches. Section 4 presents the key results, focusing on the data sampling, the model interpretation, and applicability. Finally, we discuss the findings, including a comparison with a benchmark model, and conclude in Sections 5 and 6 with an outlook on future research directions.

2. Materials

2.1. Study area

Located in the Eastern Alps, South Tyrol covers about 7,400 km², constituting the northernmost province of Italy. Its landscape is characterized by substantial heterogeneity in geomorphology, geology, land cover, and climate. The altitudinal gradient ranges from ~3900 m above sea level (a.s.l.) in the highest peaks to ~200 m a.s.l. in the narrow valley bottoms (see Figure 1). The geological settings are marked by the Periadriatic Line, the major tectonic fault that delineates the metamorphic-dominated Austroalpine section from the carbonate sedimentary-dominated Southalpine section (Stingl & Mair, 2005). The land use consists of ~40% forest, mainly on hillsides, ~35% agricultural land, prevalent in flat terrain, and the remaining ~25% corresponds to unproductive land (Autonomous Province of South Tyrol, 2021). The climate conditions exhibit strong seasonal and spatial variations, with mean annual precipitation spanning from ~500 mm in the western inner valleys to ~1,500 mm in the northern and northeastern highlands. Seasonal variation manifests in the wettest months during summer and in the driest ones during winter. The mean annual temperature ranges from approximately +15°C in the southern lowlands to around -10°C on the highest peaks, with the warmest conditions occurring in July, while the coldest ones arise in January (Crespi et al., 2021).

The specified physiographical attributes render South Tyrol predisposed to landslides, with a predominant occurrence of falls, slides, and flows. In terms of shallow slides, previous research highlighted intense or prolonged precipitation as the main triggering factors, but topography, material, vegetation cover, and land use also contribute to slope instability (de Vugt et al., 2024; Moreno et al., 2024; Piacentini et al., 2012; Schlögel et al., 2020; Steger et al., 2023; Tasser et al., 2003).

2.2. Data

2.2.1. Landslide inventory

This study relies on data sourced from the Italian landslide inventory (Inventario dei Fenomeni Franosi in Italia; IFFI), accessible through the IdroGeo platform (Iadanza et al., 2021; https://idrogeo.isprambiente.it/). In South Tyrol, the point-based information explicitly denotes the locations of field-mapped landslide scarps (Trigila et al., 2010). As of the latest access in November 2022, the inventory documented 11,944 landslides, with roughly 40% categorized as falls/topples, 35% as slides, and 15% as flows. As described in Steger et al. (2021b), the landslide data systematically captures damage-causing and infrastructure-threatening events that prompted intervention by the provincial authorities, while events without such interventions are usually not reported. This implies that landslide occurrences are underrepresented far from infrastructure.

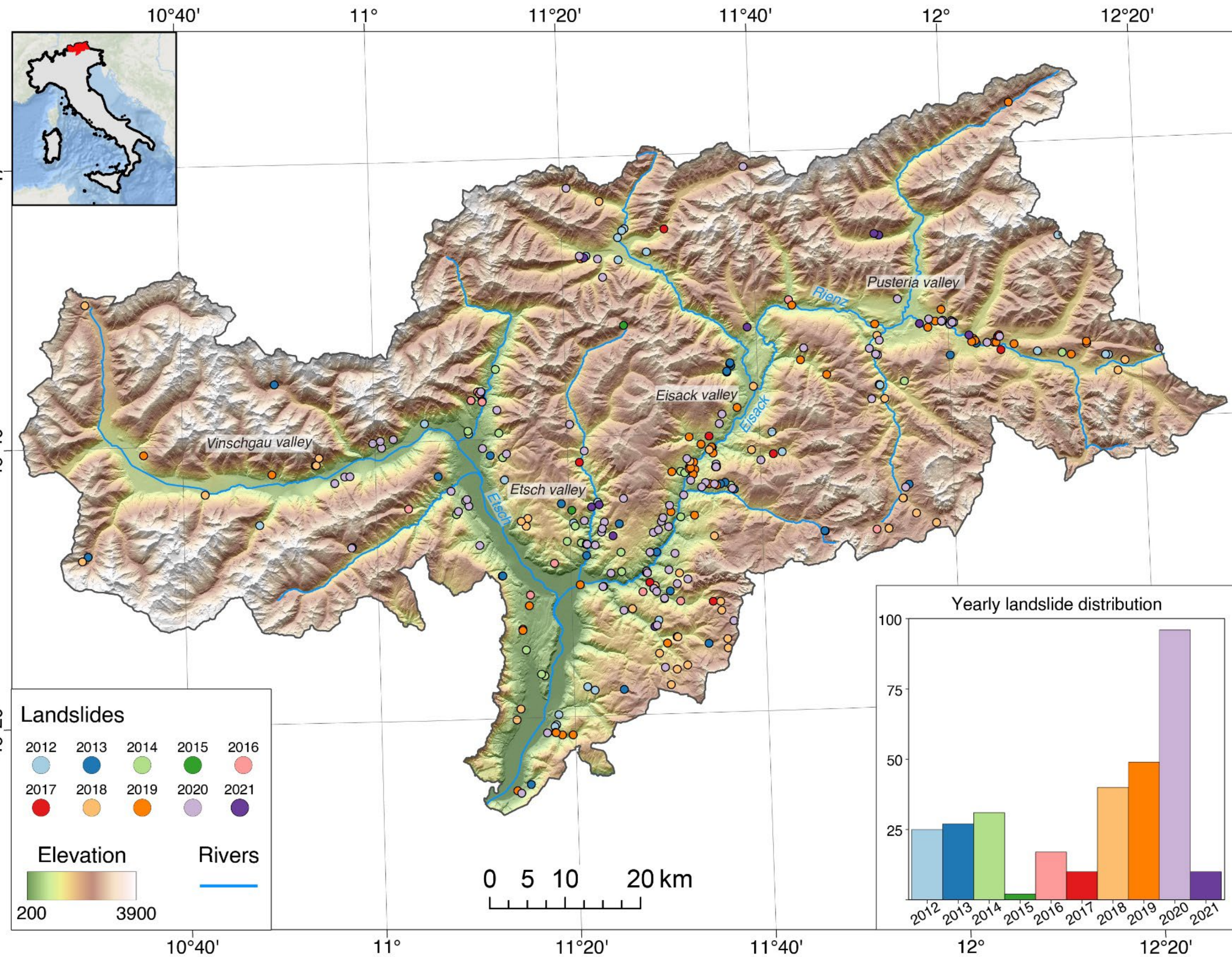

186 *Figure 1 Study area showing the elevation and the distribution of the filtered landslide scarp locations thought the years (n = 307).*

Additionally, an independent landslide inventory mapped in de Vugt et al. (2024) from high-resolution space-borne remote sensing information was considered. The 55 landslide entries were generated using multispectral imagery by PlaneScope and RapidEye to investigate the mass movements triggered by a storm event on August 4th and 5th, 2016, in the Passeier Valley, a basin located in the northwestern part of the study area.

2.2.2. Geo-environmental factors

Static factors

Identifying areas prone to landsliding through data-driven approaches hinges on analyzing spatial environmental variables observed at locations with landslides and those without. Numerous contributions elaborated on understanding the different predisposing factors and their role in slope instability (Reichenbach et al., 2018). For this study, we focused on predictors whose interpretation can provide insights into the shallow landsliding processes. Two morphometric variables were derived from a resampled LiDAR-DTM at a 30 m x 30 m spatial resolution. *Slope steepness*, a key variable in landslide susceptibility modeling, captures the gravitational forces influencing the sliding potential (Budimir et al., 2015; Westen et al., 2008). The relative elevation indicates altitude-dependent environmental and climatic conditions associated with slope instability; therefore, it is quantified via the *standardized height* provided in SAGA GIS (Conrad et al., 2015; Dietrich & Böhner, 2008). *Lithology* to describe the underlying material composition was extracted from the regional geological chart illustrating five main classes: crystalline, porphyry, sedimentary, plutonic, and calcschist ('Geologische Übersichtskarte Südtirol'; Geokatalog, 2019). A proxy for vegetation effects is the *land cover* grouped into six classes: agriculture, forest, infrastructure, pasture, rock and water/glacier ('Realnutzungskarte Südtirol v. 2015'; Geokatalog, 2019), subsequently used to create a binary *forest cover* map. Ultimately, *mean annual precipitation* from 2000 to 2020, derived from the daily precipitation grids in Crespi et al. (2021), was used to capture the overall climatic patterns and describe relatively drier and wetter areas.

Dynamic factors - gridded precipitation data

Hourly precipitation data were extracted from the Integrated Nowcasting through Comprehensive Analysis (INCA; Haiden et al., 2011), publicly released by GeoSphere Austria. INCA is a multivariable analysis and nowcasting system that offers near-real-time analyses and forecasts of variables such as precipitation, temperature, wind, humidity, and cloudiness. The INCA precipitation analysis, available since March 2011, provides data on a 1 km x 1 km spatial grid with a 15-minute temporal resolution. It integrates inputs from ~250 semiautomated weather stations, five Austrian C-band radars, and high-resolution topography. Although the precipitation measurements primarily reflect rainfall, they may also include snowfall during winter. The dataset used in this research was accessed via the GeoSphere Austria web platform (https://data.hub.geosphere.at/dataset/inca-v1-1h-1km) at a 1-h temporal resolution. For more details on the generation and processing of the INCA precipitation analysis product, refer to Ghaemi et al. (2021) and Haiden et al. (2011). One of the key advantages of using a spatially distributed nowcasting system with high-resolution radar input is its ability to provide a more accurate spatial representation of precipitation. This is critical for effectively assigning the precipitation time series and designing our modeling framework, as highlighted in Marra et al. (2014, 2016).

3. Methods

The methodical workflow is shown in Figure 2, with details outlined in Sections 3.1 to 3.4. Our model is based on binary data (i.e., landslide presences and absences), which is why the first step, *data sampling,* consisted of filtering the information from the landslide inventory (i.e., landslide presences) and strategically selecting the landslide absences. This selection included generating the Effectively Surveyed Area (ESA; Bornaetxea et al., 2018) to spatially constrain the absence sampling to well-investigated and non-trivial terrain. The combination of landslide presences and absences in space and time forms the initial model sample, which is subsequently used in the second step, *data extraction,* to obtain the associated static and dynamic environmental factors. The third step, *data modeling*, involved data-driven modeling via a binomial Functional Generalized Additive Model (FGAM; McLean et al., 2014) to predict landslides using flexible nonlinear predictors based on the temporal patterns observed before their potential occurrence. *Model evaluation* included plausibility checks, variable importance, multiple cross-validation routines, and a demonstration through hindcasting of a storm event that triggered shallow landslides in the Passeier Valley on August 4th and 5th, 2016.

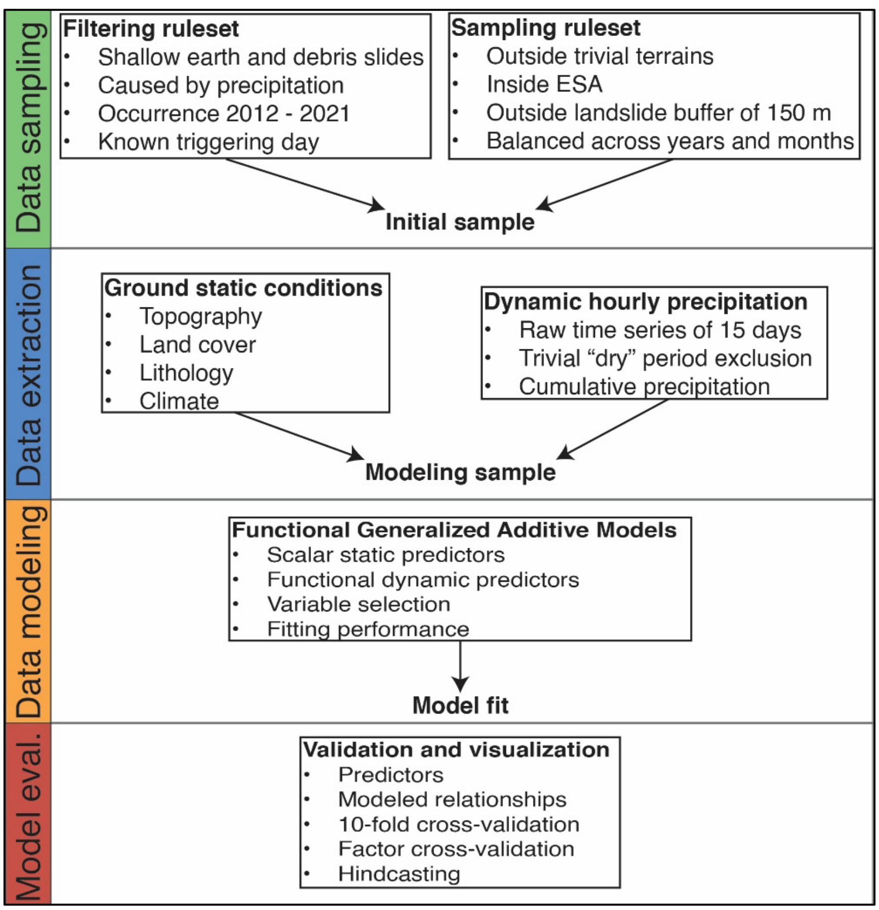

Figure 2. Overview of the implemented methodical approach.

3.1. Landslide data filtering and absence sampling

Landslide presences

The landslide inventory was narrowed down by applying four main criteria: *movement type, material type, cause type, and triggering date availability.* Additionally, we performed the analyses on data from March 2012 to December 2021. Although the INCA precipitation data are available since March 2011, the study area was not consistently covered during the first months. Consequently, we opted to restrict the analysis period to begin in March 2012 to ensure consistent data coverage.

Landslide absences

Ensuring an appropriate selection of landslide absence data is equally critical as selecting the landslide presence data. Notably, sampling landslide absences presents a more complex challenge, as it requires the strategic definition of areas and periods where and when landslides are presumed not to occur. Additionally, because binary classification models are sensitive to the ratio between landslide presences and absences, systematic biases can be introduced if either presence or absence data are strongly underrepresented or overrepresented (Steger et al., 2017).

We considered two key components to construct the landslide absence sample in space: the ESA mask and the exclusion of trivial terrain. Effectively Surveyed Area represents the areas explicitly surveyed while mapping the landslide inventory. We generated the ESA mask to mitigate misleading correlations due to systematic biases arising from the uneven representation of past landslides (Bornaetxea et al., 2018; Steger et al., 2021). In other words, this mask restricts the sampling area to ensure that absence observations are only considered within well-observed terrain. This mask is built upon factors such as the proximity to infrastructure (e.g., buildings, roads, railways, pathways) and elevation. This procedure to generate the ESA mask has been comprehensively detailed in Steger et al. (2024). The trivial terrain consists of easy-to-classify areas where no landslides are expected (Steger & Glade, 2017). We identified rocky faces, glaciers, water bodies, and flat lands as trivial terrains to be excluded from the sampling area. The trivial terrains and ESA criteria were equally applied to the landslide presences to keep the sampling strategy consistent. Furthermore, we included a minimal distance to known landslide locations of 150 m as an additional criterion within the filtering ruleset.

Landslide absence locations were randomly selected within the defined sampling area, with each location being assigned a randomly chosen date between March 2012 and December 2021. The selection was constrained to achieve balanced yearly and monthly distributions to ensure a uniform temporal distribution of landslide absences. This initial dataset underwent further filtering by applying a precipitation threshold to exclude dry days from the analysis, as detailed in Section 3.2.

3.2. Precipitation time series

After obtaining the initial dataset comprising the spatiotemporal distribution of landslide presences and absences, we extracted the environmental data. The static or scalar predictors were extracted directly using the sample location and the gridded datasets mentioned in Section 2.2.2. Additionally, predictors such as the *year*, *month*, and *day of the year (doy)* were derived from the assigned observation dates.

Precipitation data, as the functional predictor, was extracted from the INCA dataset for each observation using the sample locations and the assigned observation dates. Following the findings in Moreno et al. (2024), hourly precipitation time series were built up to 15 days prior to the observation dates. Similarly to trivial terrains, we defined trivial periods based on a precipitation threshold so that observations with no precipitation amounts ≥ 1 mm on any of the last 72 hours, including the observation day, were excluded from further analysis. This step focuses the problem on predicting precipitation-induced landslides in wet conditions and prevents the model from simply learning the difference between dry and wet conditions. With this procedure, additional landslides not primarily caused by precipitation, such as human interventions, could be excluded. Finally, the precipitation time series were represented in forward cumulative precipitation for each observation, so the last hour at the observation date (day 0 – hour 0) contains the total precipitation over the previous 15 days or 360 hours.

3.3. Functional Generalized Additive Models

Theoretical background

Generalized additive models (GAMs) are flexible statistical approaches that estimate relationships between a response variable and a set of predictors. Unlike traditional models that assume linear associations, GAMs are designed to handle a wide range of error distributions and account for nonlinear associations between the predictors and the response. This is achieved by allowing each predictor to have its smooth function, enabling the model to capture complex underlying patterns flexibly. This adaptability is particularly advantageous when linear functions cannot adequately describe the relationships between predictors and the response (Bolker et al., 2009; Pedersen et al., 2019; Wood, 2017; Zuur et al., 2009).

One of the major strengths of GAMs is their interpretability. The smooth functions provide clear insight into the nature of their effects, making it easier to understand how each predictor influences the response. Moreover, GAMs can be extended to model interactions between predictors, providing greater flexibility in modeling complex relationships. Due to their high interpretability and flexibility, GAMs have become widely used across many scientific disciplines, including landslide modeling (Ahmed et al., 2023; Camera et al., 2021; Lin et al., 2021; Lombardo et al., 2020; Moreno et al., 2023). GAMs further allow for probabilistic uncertainty assessment through confidence bounds of the predictions and estimated partial effects of the predictors.

Functional data analysis (FDA) is a statistical framework developed to analyze data recorded as functions over a continuous domain, such as time (Ramsay & Silverman, 2005). In contrast to traditional methods, which focus on scalar observations, the FDA considers functions to be the fundamental units of analysis. This approach is particularly useful in settings where the data is expressed as time series with non-negligible temporal correlation or specific temporal patterns that help to improve interpretation and prediction. Various methods have been developed within this broad framework, including functional regression models, where the response or predictors are treated as functional data (Morris, 2015). In this context, scalar-on-function regression is a common approach, where the response variable is scalar, and the predictors are functional, meaning that predictors are represented as functions rather than a single value.

Building upon these approaches, functional generalized additive models (FGAMs), as presented in McLean et al. (2014), extend the flexibility of GAMs by incorporating the strengths of the FDA. FGAMs allow for the inclusion of both scalar and functional predictors in a single model, making it possible to model the effect of time-varying predictors on a scalar response. Similarly to GAMs, FGAMs facilitate the modeling of complex nonlinear relationships while allowing functional predictors to be treated as smooth curves or surfaces. FGAMs achieve this by decomposing those functional predictors into smooth basis functions, which are then integrated over the functional domain, enabling the model to account for time-varying and time-lagged effects on the response variable. The flexibility and interpretability of FGAMs, inherited from the GAMs, make them particularly valuable in scenarios where temporal dependencies are critical, such as spatiotemporal modeling.

Model fit

The model fit was performed via the tools implemented in the comprehensive R package *refund* (Goldsmith et al., 2024; McLean et al., 2014). This package allows the fitting of penalized scalar-on-function regression models, where, in our case, the scalar binary response is the presence (or absence) of landslides, and the functional predictor is the hourly precipitation time series in a fixed-length segment preceding the time of the observed response.

Predictor assessment and selection were carried out through variable importance analysis and the evaluation of modeled relationships. Variable importance analysis gives insights into the relative contribution of each predictor to the response variable. In the FGAM, predictors were ranked based on the estimated proportion of deviance explained, a well-known measure of the goodness of model fit. We compared the deviance explained by a full model (i.e., including all the predictors) against a series of reduced models, each omitting a specific predictor. A larger reduction in deviance explained indicates a greater relative contribution of the corresponding predictor of interest (Goetz et al., 2018). Partial effect plots were used to illustrate how the estimated landslide probabilities change in response to variations in individual predictors, providing a means to assess the plausibility of the modeled relationships. For the case of the functional predictor, the partial effect plots were visualized as contour plots to represent the nonlinear interactions between *precipitation time series*, time, and the response variable.

3.4. Model validation and visualization

For model evaluation, we employed a set of well-established diagnostic tools. The model performance was assessed using the R package *sperrorest* (Brenning et al., 2022) through several approaches: k-fold random cross-validation (RCV), k-fold spatial cross-validation (SCV), temporal cross-validation (TCV) based on both *years* and *months* and leave-one-factor-out cross-validation (FCV) using *lithology*.

Random cross-validation involves repeatedly partitioning the available dataset into disjoint training and testing sets, in our case, using ten folds and ten repetitions, resulting in 100 iterations (Brenning, 2012). The area under the Receiving Operator Characteristics curve (AUROC) was computed for the independent testing sets to assess the predictive performance for each partition. The ROC curve graphically represents the performance of a binary classifier by varying the discrimination threshold. At the same time, the AUROC value usually ranges from 0.5 (i.e., random classification) to 1 (i.e., perfect discrimination), with higher values indicating a better-performing model (Hosmer et al., 2013). Conventional RCV routines may fail to capture the spatial variability of the model performance, potentially leading to over-optimistic results if the spatial model predictions poorly align the data within a specific subregion of the study site. Thus, we applied SCV, which can be used to estimate the spatial transferability of the model and reveal spatially incoherent predictions. This study's underlying spatial partitioning approach was achieved through a k-means clustering approach, with ten folds and ten repetitions, mirroring the RCV setup.

We also applied TCV and FCV to assess model transferability across time and lithological units in addition to the cross-validation routines described earlier. Temporal cross-validation was performed by iteratively excluding observations from either one month (leave-1-month-out) or one year (leave-1-year-out) from the training dataset. This was followed by evaluating the model predictions on the excluded data using the AUROC. Similarly, FCV was applied using the five different lithological units to define the training and testing datasets.

For visualization purposes, we used our dynamic model in a demonstration test. Ideally, the model can simulate any day of the year, given the availability of precipitation data prior to that day. To illustrate its practical application, we conducted a hindcast for the landslides triggered by the storm event on August 4^{th} and 5^{th}, 2016, in the Passeier Valley using the precipitation time series for those respective dates. The estimated model predictions were then compared to the landslide inventory mapped in de Vugt et al. (2024), which documented the same storm event.

4. Results

4.1. Landslide data sampling

After applying the first filtering ruleset, the initial 11,944 landslide observations in the IFFI dataset were narrowed down to 338 *shallow earth and debris slides* caused by *short-intense and prolonged precipitation* with a known triggering day between March 2012 and December 2021. This subset was refined by excluding observations located within trivial terrain and outside the ESA, resulting in 307 landslide records. Similarly, a precipitation threshold was applied to exclude trivial periods, retaining only observations with precipitation exceeding 1 mm during the 72 hours preceding the landslide date. We obtained a final sample size of 259 landslide observations following this final filter.

The combination of the landslide presence and absence samples resulted in a total of 6,448 observations (Figure 3a), with 6,138 corresponding to landslide absences, yielding a ratio of approximately 1:20 in terms of landslide presences and absences, respectively. The temporal distribution of absences was kept uniform across years and months. In particular, the initial monthly absence sample was proportional to the number of days each month. After using the precipitation threshold to exclude the trivial periods, we obtained a final modeling sample that only included the days with precipitation exceeding 1 mm during the last 72 hours before the observation day, resulting in a total of 3,233 observations. This final sample comprised 259 landslides and 2,974 absence samples, representing a ~50% reduction from the initial dataset and an updated presence-to-absence ratio of about 1:10. Notably, 48 landslide observations were removed potentially because they were not primarily caused by precipitation. Since we entirely removed non-ESA locations and times with preceding negligible precipitation activity from the dataset, the landslide occurrence probabilities estimated by the model we implement must be interpreted conditionally to being within the ESA region and the presence of preceding precipitation. Achieving good predictive scores of the model is more challenging in this setting since trivial conditions are removed. On the other hand, it is also facilitated since some noisy observations, i.e., landslides occurring in trivial conditions with triggers other than precipitation, are also excluded.

Figure 3b shows that observations with precipitation were relatively more frequent during summer months (i.e., May, June, July, and August). Although November had fewer 'wet' days, it exhibited the highest frequency of landslides, suggesting a seasonal influence consistent with the findings in Steger et al. (2023).

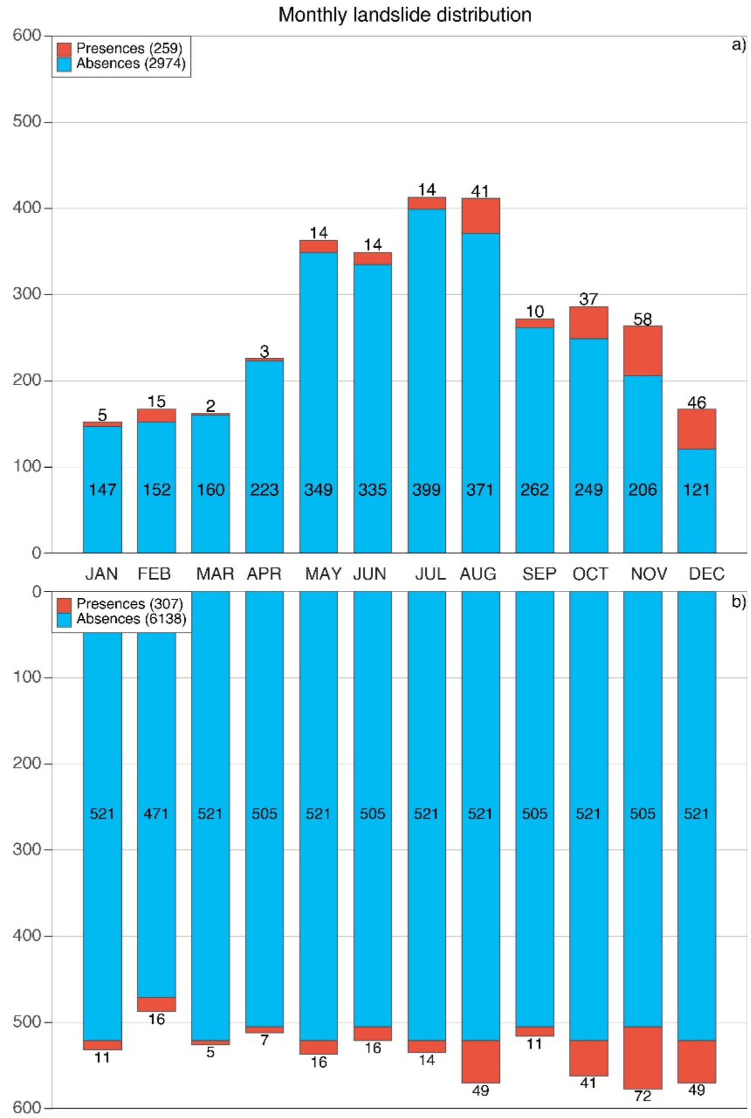

Figure 3. Data sampling results. The bar plots show the monthly frequency of the sampled data before (a) and after (b), excluding the trivial periods. Landslide presences are colored red, while the absences are in blue.

4.2.Precipitation time series

Based on the previously constructed dataset, we extracted static geo-environmental factors and precipitation time series data. After applying the precipitation threshold, Figure 4a shows the average precipitation across hours and the corresponding 95% confidence interval for landslide presences (in red) and absence samples (in blue) for the 3,233 observations. Overall, landslide presence samples experienced, on average, higher hourly precipitation than absence samples over the 15-day analysis period. The differences became particularly pronounced between days 0 and 5, with landslide samples typically showing time stamps with approximately 1.5 mm more precipitation on average than absence samples.

The analysis using cumulative precipitation for each event in Figure 4b further highlighted these differences, with up to 100 mm more precipitation observed for landslide presences than absence observations during days 0 to 5. Given the smoother and more stable nature of the cumulative precipitation signal, as opposed to the more erratic fluctuations of hourly precipitation, we opted to use cumulative precipitation data from day 0 up to day 5 for the subsequent modeling procedures. These differences are highlighted during the discussion in Section 5.

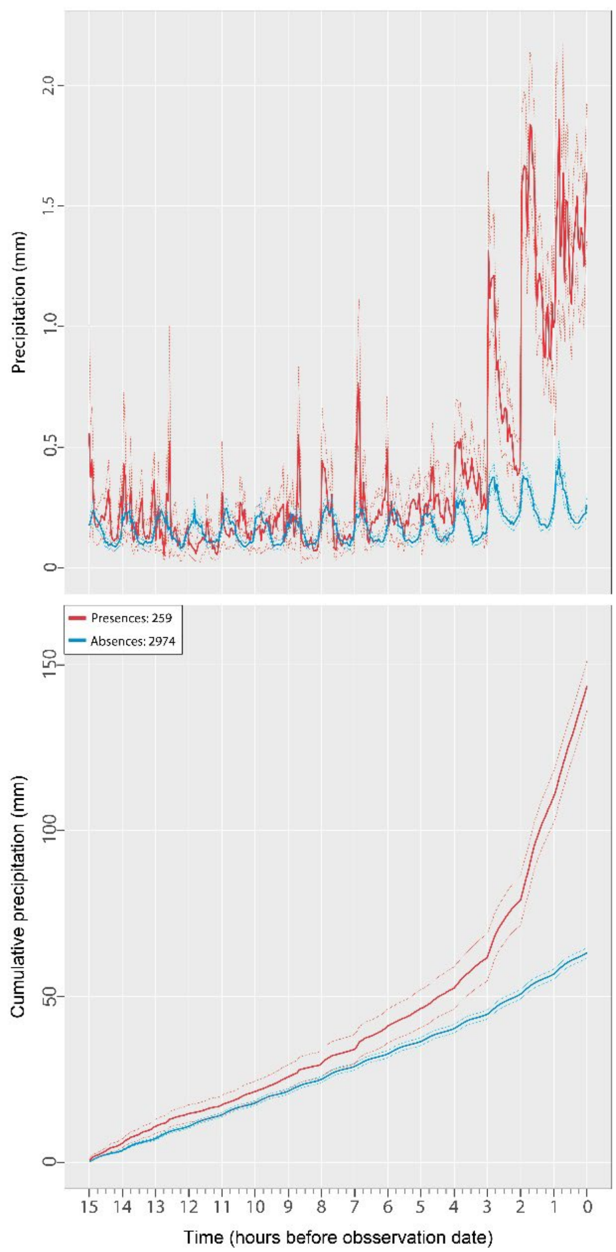

Figure 4. Precipitation time series extraction. The plots show the average hourly time series of precipitation (a) and cumulative precipitation (b) in solid lines, with the 95% confidence interval in dotted lines for landslide presences (in red) and landslide absences (in blue) up to 15 days before the observation date.

4.3. Model fit and model relationships

We performed the model fit iteratively. The non-reported iterations were evaluated regarding the significance of the predictors and the plausibility of the partial effect plots, leading to the final model fit, as summarized in Table 1, along with other details on the FGAM parametrization. The relative contribution of each predictor was determined through variable importance analysis, with a higher proportion of deviance explained, indicating a higher contribution to the model. All the selected predictors increased the deviance explained by the model, with the *precipitation time series* (0.282) emerging as the most important factor in predicting landslide occurrence. The topographic predictors, such as the *slope steepness* (0.065) and the *standardized height* (0.029), also showed relevant contributions. In contrast, the *lithology* (0.006) and the *doy* (0.003) had much less influence on the occurrence of landslides.

Table 1. Model setup. Predictors introduced in the binomial FGAM and their variable importance. The tensor product smooth function of the cumulative precipitation series captures the interaction of hourly time lag and precipitation (with thin plate spline bases for each of these two dimensions), contributing to possible landslide occurrence.

Predictor	Deviance explained	Smooth function	Significance (p-value)	
Cumulative precipitation time series	0.282	Tensor product	<0.001	
Slope	0.065	Thin plate spline	<0.001	
Standard height	0.029	Thin plate spline	<0.001	
Forest	0.013	Factor term	No	Ref. level
			Yes	<0.001
Mean precipitation	0.012	Thin plate spline	0.002	
Lithology	0.006	Factor term	Crystalline	Ref. level
			Porphyry	0.239
			Sedimentary	0.084
			Plutonic	0.508
			Calcschist	0.033
Doy	0.003	Cyclic cubic spline	0.063	

The partial effect plots provided a clear summary of the modeled relationships. Figure 4a illustrates that the estimated regression coefficients (RC) generally increase as cumulative precipitation rises and time progresses, peaking on the final observation day for cumulative precipitation amounts exceeding 100 mm.

Figure 5b-e depicts how estimated landslide probabilities vary with changes in *mean annual precipitation*, *doy*, *slope steepness*, *standard height*, *forest*, and *lithology*. For instance, *mean annual precipitation* indicates higher landslide probabilities in relatively drier areas (600–900 mm), while wetter regions (1100–1400 mm) show low probabilities. Regarding *doy*, the analysis reveals slightly reduced probabilities around *doy*$_{200}$, corresponding to mid-July, the summer season. Topographic predictors, such as *slope steepness,* exhibit a parabolic trend, with lower landslide probabilities at 0° inclination, reaching its maximum at ~30° and diminishing for slopes up to ~60°. In the case of the *standard height*, the landslide probabilities show a nonlinear trend, with probabilities gradually decreasing as the height values increase.

Categorical predictors presented in Figure 5f-g included the *land cover* and *lithology*. The different land cover classes were iteratively tested, and the class that showed plausible and statistically significant results was simplified to a binary predictor: the presence or absence of *forest*. These results show that the *forest* presence negatively influences the occurrence of landslides. For *lithology*, the classes that showed statistical significance (with reference to class *crystalline*) were *sedimentary* and *calschist,* with *sedimentary* rocks associated with positive RC and *calschist* with negative coefficients.

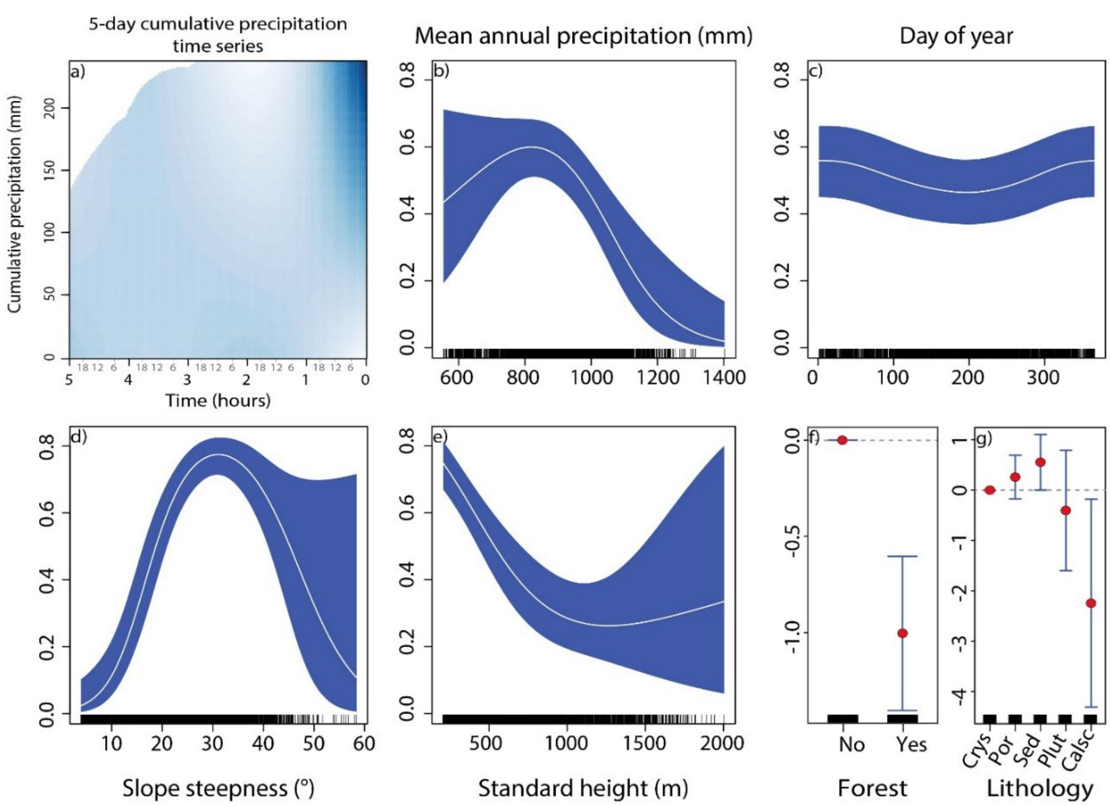

Figure 5. Partial effect plots. Panel a shows the interaction effect of the cumulative precipitation time series and time, with the y-axis expressing the cumulative precipitation, the x-axis representing the time in days and hours, and the colors representing the regression function (darker color for higher values). In panels b, c, d, and e, the center lines in white show the mean estimated effect,

and the blue bands show the associated 95 % confidence interval, with the y-axis expressed at the response scale. Panels f and g show the mean estimated effect (red dots) with the associated 95% credible interval with the y-axis expressed at the linear scale.

4.4. Model evaluation and visualization

The cross-validation routines outlined in Figure 6 demonstrate a relatively high model generalization and transferability, with AUROC scores consistently exceeding 0.90, indicating *outstanding discrimination* as defined in Hosmer et al. (2013). The two 10-fold cross-validation strategies (Figure 6a) RCV and SCV yield median AUROC values of 0.929 and 0.927, respectively. As expected, SCV using k-means clustering shows slightly lower performance with a wider interquartile range (IQR) compared to RCV, as SCV reduces residual dependence from the spatial dataset, providing a less biased evaluation of the predictive capability.

Leave-one-out cross-validation routines, such as TCV (for years and months) and FCV (for lithology) in Figure 6b-d, show mean AUROC values of 0.881, 0.885, and 0.937, respectively. Lower performance scores in specific years, months, and lithological units likely reflect variations between the conditions driving landslide occurrences in these units and those captured in the model, which was trained on the remaining units. TCV for years and months demonstrates robust temporal transferability, with performance scores slightly lower for 2017 and 2016 and higher for 2019, 2018, and 2015. At the monthly level, lower performance scores are observed in May and September, likely due to abrupt changes in precipitation patterns: an increase during the transition from April to May and a decrease during the transition from September to October (Crespi et al., 2021). In contrast, the period from October to March shows the highest AUROC values. On the other hand, FCV reveals AUROC values above 0.9 for all lithological classes except *sedimentary*, which scores ~0.85. This indicates that the modeled relationships are generally well transferred across the lithological units with lower performance for the *sedimentary* units.

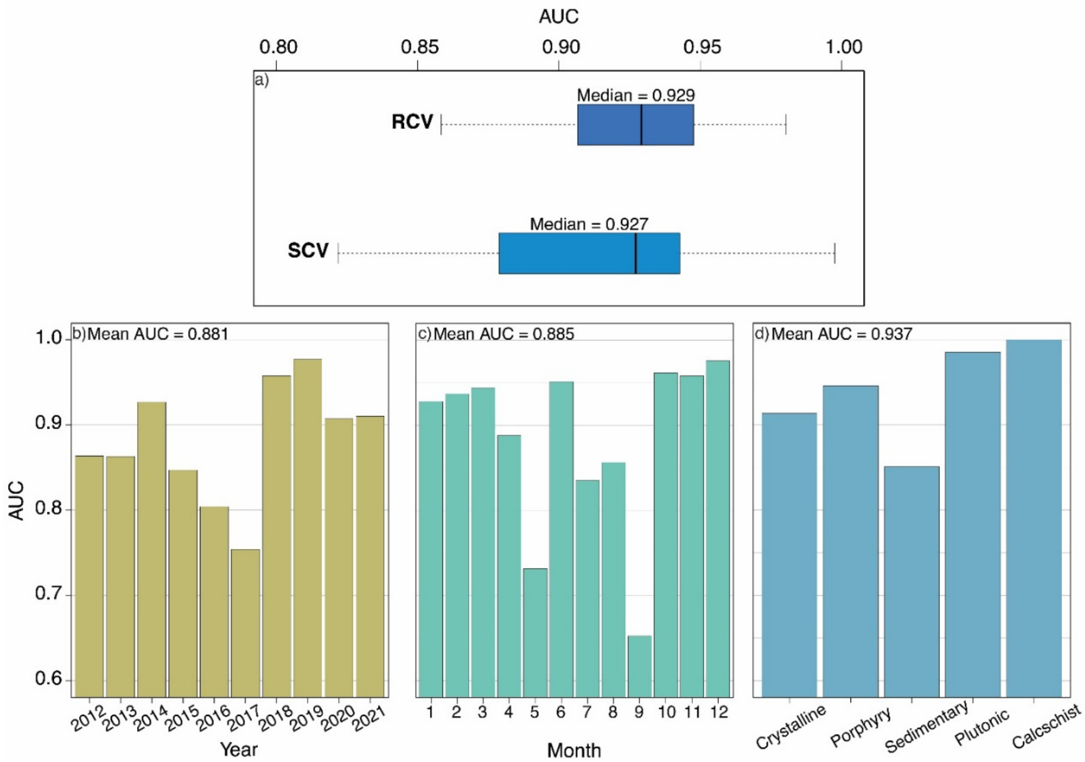

Figure 6. Summary of the model performance. Panel a shows the 10-fold RCV and 10-fold SCV, whereas the remaining panels show the TCV for years and months and FCV for the lithological classes.

For visualization purposes and to demonstrate the predictive capabilities of the model, we applied the model to hindcast the landslides triggered during a storm event that took place in the Passeier Valley on August 4th and 5th, 2016. This localized storm event was characterized by strong precipitation that triggered numerous landslides in the catchment of the Passeier River, making it a suitable case study to evaluate the predictive capabilities. The resulting predictions are stored as an animation GIF file, *Passeier_Timeseries_GIF.gif,* and provided in the supplementary materials.

Furthermore, Figure 7 displays a selection of four specific frames from this animation file, focusing on the critical period from 03:00 to 21:00 on August 5th. These frames illustrate both the hourly precipitation data, sourced from the INCA dataset, alongside the corresponding landslide probabilities generated by the model. Examining these frames makes it possible to observe how the landslide probabilities evolve dynamically in response to increasing precipitation over time. At the onset of the selected time interval (03:00) when the precipitation peaks, the model predicts relatively low landslide probabilities across the affected area. However, as time progresses and the cumulative impact of precipitation becomes more pronounced, the predicted landslide probabilities increase. By 15:00, the model indicates moderate landslide probabilities, particularly near the main valley bottom, which subsequently peaked at 21:00, revealing high landslide probabilities in the area of interest.

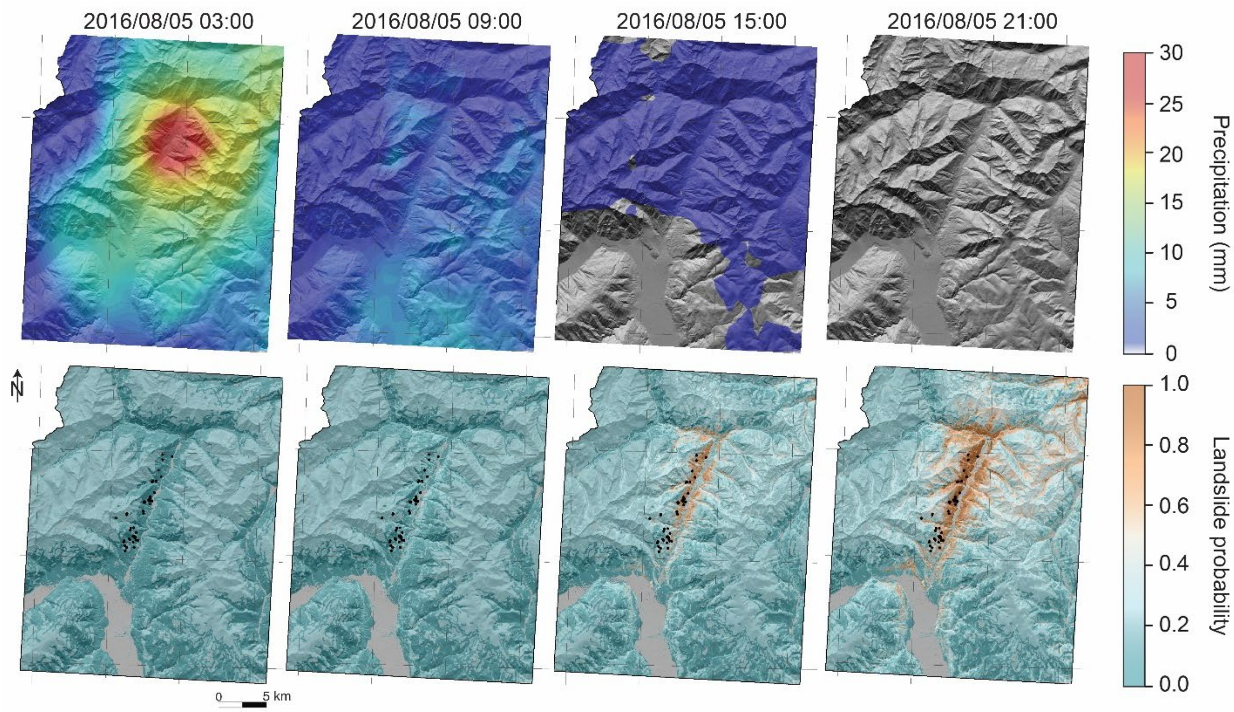

Figure 7. Extract of the dynamic landslide predictions for hindcast on landslides associated with the precipitation event in the Passeier Valley on the 4th and 5th of August, 2016. The first row shows the precipitation amounts on August 5th from 03:00 UTC to 21:00 UTC, whereas the second row shows the associated landslide predictions. The black points correspond to the independent landslide inventory mapped in de Vugt et al. (2024).

5. Discussion

In this study, we implemented a space-time classification framework that integrates static scalar and dynamic functional factors to predict the occurrence of precipitation-induced shallow landslides. The proposed model exhibits strong predictive performance, regularly achieving AUROC scores surpassing 0.90. This indicates the ability of the model to account for various influencing factors, including static ground conditions, precipitation as a function of time, seasonal effects, and spatial biases. The model's strengths and limitations are discussed below.

Before diving into the details of model strengths and limitations, it is relevant to address a key aspect of space-time landslide predictive modeling. Most current space-time models treat space continuously, while time has mostly been treated discretely, either according to even-based inventory dates or aggregated over extended periods such as years or seasons (Ahmed et al., 2023; Dahal et al., 2024; Wang et al., 2022). In contrast, our model preserves time in its original continuous daily resolution for landslides and hourly for precipitation, a strategy that inevitably leads to several orders of magnitude larger numbers of landslide absences than the presence sample. Modeling such a daily spatiotemporal domain is impractical; hence, we devised a sampling design to uniformly capture spatiotemporal variability of presence-absence conditions while excluding trivial and potentially biasing information from the data. This approach involved applying several key rules, namely: i) masking out trivial terrains (Steger & Glade, 2017), ii) sampling exclusively within the effectively surveyed area (Bornaetxea et al., 2018; Steger et al., 2024), iii) excluding samples within a 150 m radius of each landslide location, iv) balancing absence samples across years and months, and v) masking out trivial time periods. We recommend analogous considerations and present the current protocol as a blueprint for future studies with similar space-time data structures.

Beyond performance-oriented considerations, models that treat precipitation as a continuous signal offer the inherent advantage of bypassing the need for arbitrary aggregation choices over time. In other words, no expert choice is needed; rather, the data-driven tool of choice finds the best functional relations. Conversely, space-time solutions treating precipitation as a scalar predictor require a preprocessing step where the model iteratively evaluates various time windows to determine the most suitable representation (Gómez et al., 2023; Moreno et al., 2024; Nocentini et al., 2023; Smith et al., 2023). Another key feature of our model is its ability to inherently use the whole time series to estimate and account for lagged precipitation effects. This allows the model to incorporate delayed responses in its predictions. As shown in Figure 7, and the supplementary animation *Passeier_Timeseries_GIF.gif*, the model reveals how the initial precipitation amounts do not immediately produce an equivalent raise in the dynamic landslide probabilities. Instead, this increase occurs much later in the simulation when the lagged precipitation contributions become relevant and added to subsequent precipitation.

We highlight our model's high interpretability and obtained performance, though the interpretation of the modeled relationships was not fully detailed within this work. The strong flexibility and interpretability are largely due to using an FGAM framework. Particularly, variable importance assessment and the partial effect plots provide valuable insights into the statistical contributions of both scalar static and functional dynamic environmental factors to landslide occurrence across space and time. Consistent with classification standards in Hosmer et al. (2013), the model shows *outstanding discrimination* capabilities, supported by multiple implemented cross-validation routines across space, time, and environmental factors.

We believe the model holds the potential for advancing LEWS. However, we also recognize that it is currently far from being ready for operational purposes. This is mainly because calculating the functional predictor is inherently time-consuming due to the large number of elementary arithmetic operations required. Such an intensive task was conducted on the ITC geospatial data analysis platform (CRIB; https://crib.utwente.nl/), using a computing setup equipped with 72 vCPUs (Intel x86–64), 768 GB of RAM, and an NVIDIA RTX A4000 GPU. This limitation poses a critical barrier, as effective EWS deployment requires seamless nowcasting and forecasting of landslide occurrence probabilities. Under the current setup, several data conversions and I/O operations are required, resulting in a rather lengthy and slow process. Beyond computational considerations, we acknowledge challenges in applying this framework for forecasting purposes since the forecasted precipitation amounts would need to be elaborated further into time series to enable landslide predictions. While it is acceptable and manageable for research, new and more flexible computational strategies are essential to meet the demands of real-time operational systems.

We emphasize that while our developed approach incorporates a proxy such as the *doy*, it does not account for the effects of antecedent precipitation conditions or soil moisture preceding the slope failure. For shallow landslides, antecedent soil moisture is critical in regulating rainwater infiltration and ultimately triggering slope failure (Greco et al., 2023). In our analysis, the use of hourly time series spanning five days and *doy* does not adequately capture these conditions. We recommend that future studies explore the inclusion of antecedent soil moisture in such a modeling framework. At regional scales, soil moisture estimates are typically derived from satellite products (Thomas et al., 2019), with in situ measurements being used much less frequently (Wicki et al., 2020).

A critical point for consideration—and one that may invite critique — concerns benchmarking our results against a space-time model designed according to the standards for EWS. A traditional EWS relies solely on precipitation information, thus leaving aside the contribution to the prediction brought by landscape characteristics. Moreover, the use of the precipitation signal itself is aggregated to a scalar value for a specific time window of interest by computing the precipitation sum. To illustrate this comparison, we created Figure 8, where Figure 8a displays the model performance only using precipitation in its raw (blue) and cumulative (red) forms. As for Figure 8b, we reported the performance of an equivalent model to which landscape characteristics such as *slope steepness*, *lithology*, *standard height*, *land cover*, *mean annual precipitation*, and *doy* have been incorporated. Ultimately, Figure 8c depicts the performance obtained using a functional representation of the precipitation with landscape-related predictors.

What stands out is that the use of raw precipitation is consistently the wrong choice when the signal is aggregated per fixed time windows. The same cannot be said for our functional approach, where the distinction between raw and cumulative precipitation as continuous signals leads to essentially very similar results. As for the use of aggregated precipitation, interestingly, even Figure 8a shows remarkable prediction capabilities when it comes to cumulative precipitation, although it still underperforms compared to the models in Figure 8b-c. When focusing on the latter panels, we observe that our functional approach is slightly better, irrespective of how one processes the precipitation signal. Overall, scalar and functional cumulative precipitation lead to negligible variations between Figure 8b and Figure 8c that need to be acknowledged. This implies that a scalar use of the precipitation signal if it is combined with landscape properties, leads to very satisfying results. An important difference is highlighted in the work carried out in Fang et al (2023) and Lim et al. (2024), where there was an improvement in predictive power of ~20% when using only functional precipitation predictors and ~10% when using both static and functional precipitation predictors, respectively. Still, a key advantage of the functional model is its ability to leverage the entire time series, eliminating the need for cumbersome tests across various time windows —a process typical of EWS setups. This efficiency favors functional models for practical implementations, a tradeoff with computational needs.

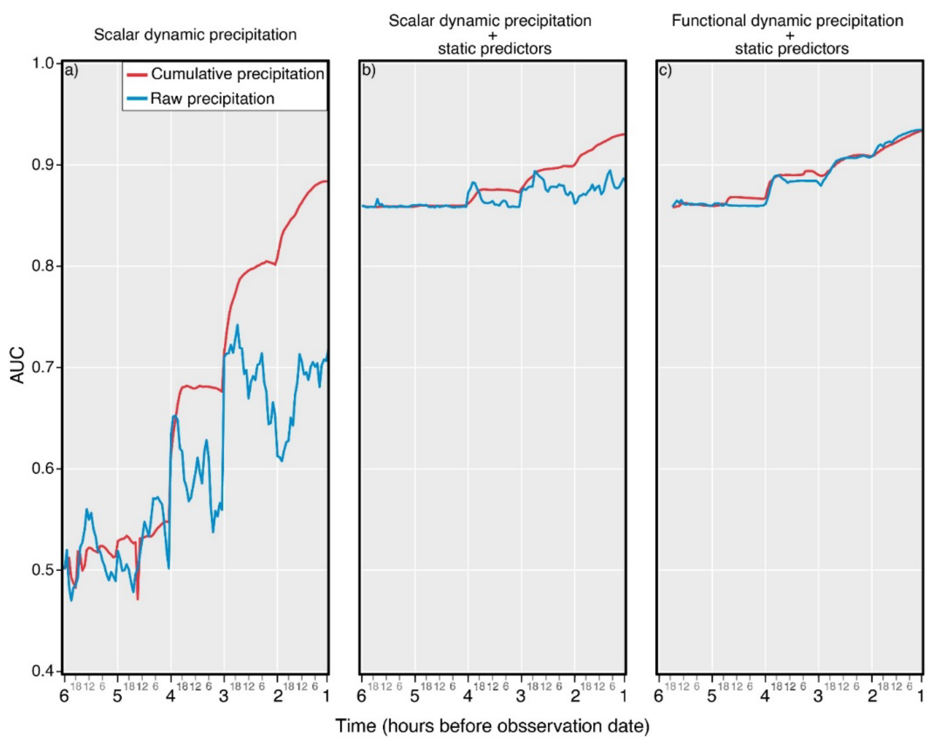

Figure 8. Illustration of the benchmark performance report. On the x-axis, the time intervals (in hours and days) for which precipitation was considered in the models, whereas the y-axis indicates the corresponding AUC scores. In each panel, blue lines represent models that use raw precipitation, and red lines represent those using cumulative precipitation. Panel a displays models using solely scalar precipitation predictors; panel b incorporates both scalar precipitation predictors and landscape characteristics; finally, panel c integrates the landscape characteristics with the precipitation in its functional representation. Note that the cumulative precipitation was computed forward in time, meaning that T_{d1h0} *(day 1 at hour 0) reflects the total precipitation over the entire period of analysis. For panel c, the time series begins 6 hours into the period (*T_{d6h18}*) and progressively extends at each subsequent timestamp until the entire time series is incorporated at* T_{d1h0}*.*

6. Conclusion

Throughout the experiments conducted in this research, several noteworthy findings emerged, particularly in comparison to standard early warning practices. A functional representation of precipitation captures lagged effects, a feature yet to be observed in the landslide early warning literature, a field of research where we will further place future efforts. Another important element is the contribution of the landscape characteristics in addition to the dynamic contribution of precipitation. Current technological advancements have made it difficult to justify using a model that relies solely on precipitation for threshold estimation and a separate model based on terrain characteristics for susceptibility estimation. Data-driven models have already achieved a degree of flexibility, and computational environments now offer sufficient resources that allow the integration of static and dynamic predictors in a single tool. This shift could lead to a fundamental change in focus from precipitation thresholds to unified landslide probability thresholds if widely accepted. We expect this will be the direction the geoscientific community will take in the coming years, with our work contributing to this potential evolution.

A functional representation of the precipitation certainly removes the need to identify the best time windows for aggregating precipitation. Still, more could be done regarding how one considers the precipitation signal. We are currently testing our functional approach with precipitation signals interpolated from rain gauge records, terrestrial radar stations, and satellite products. This is an area where we expect further differences between a functional and a scalar precipitation setup, and even more could be done by concatenating more than one likelihood. For instance, not only predicting where and when landslides may occur but also jointly predicting how large they may be.

CRediT authorship contribution statement

Mateo Moreno: Writing – original draft, Visualization, Validation, Methodology, Formal analysis, Data curation, Conceptualization. **Luigi Lombardo**: Writing – review & editing, Supervision, Methodology, Conceptualization. **Stefan Steger**: Writing – review & editing, Supervision, Conceptualization. **Lotte de Vugt**: Writing – review & editing. **Thomas Zieher**: Writing – review & editing. **Alice Crespi**: Writing – review & editing, Data curation. **Francesco Marra:** Writing – review & editing, Data curation. **Cees van Westen:** Writing – review & editing, Supervision. **Thomas Opitz**: Writing – review & editing, Supervision, Methodology, Formal analysis.

Financial support

This research has been supported by the autonomous province of Bolzano (grant no. 9/34), the Faculty of Geo-information Science and Earth Observation (ITC-UTWENTE), and the Biostatistics and Spatial Processes unit (INRAE).

Acknowledgments

The research that led to these results is related to the PROSLIDE project (https://www.mountainresearch.at/proslide/), which received funding from the research program Research Südtirol/Alto Adige 2019 of the autonomous province of Bolzano. We thank the Faculty of Geo-information Science and Earth Observation (ITC) – University of Twente for covering the open-access publication fees We thank. We thank Dr. Serkan Girgin for his support with using the CRIB platform. We thank the Office for Meteorology and Avalanche Prevention, especially Mauro Tollardo, for supporting and providing data. Finally, we thank the provincial Office for Geology and Building Materials Testing for assisting in preparing landslide data.

Code and data availability

The modeling procedure was conducted in R. The scripts are available at the repository https://github.com/mmorenoz/FGAM_LandslidePrecipitation. The landslide inventory can be accessed from https://idrogeo.isprambiente.it/app/page/open-data. The hourly precipitation data from the INCA dataset is available at https://data.hub.geosphere.at/dataset/inca-v1-1h-1km. The environmental datasets (lithological map, land cover, terrain model) can be accessed from the open geodatabase of the Autonomous Province of South Tyrol through http://geokatalog.buergernetz.bz.it/geokatalog/#!.

References

Ahmed, M., Tanyas, H., Huser, R., Dahal, A., Titti, G., Borgatti, L., Francioni, M., & Lombardo, L. (2023). Dynamic rainfall-induced landslide susceptibility: A step towards a unified forecasting system. *International Journal of Applied Earth Observation and Geoinformation*, *125*, 103593. https://doi.org/10.1016/j.jag.2023.103593

Aleotti, P., & Chowdhury, R. (1999). Landslide hazard assessment: Summary review and new perspectives. *Bulletin of Engineering Geology and the Environment*, *58*(1), 21–44. https://doi.org/10.1007/s100640050066

Alvioli, M., Loche, M., Jacobs, L., Grohmann, C. H., Abraham, M. T., Gupta, K., Satyam, N., Scaringi, G., Bornaetxea, T., Rossi, M., Marchesini, I., Lombardo, L., Moreno, M., Steger, S., Camera, C. A. S., Bajni, G., Samodra, G., Wahyudi, E. E., Susyanto, N., … Rivera-Rivera, J. (2024). A benchmark dataset and workflow for landslide susceptibility zonation. *Earth-Science Reviews*, *258*, 104927. https://doi.org/10.1016/j.earscirev.2024.104927

Autonomous Province of South Tyrol. (2021). *South Tyrol in figures. Provincial Statistics Institute*. https://astat.provinz.bz.it/downloads/Siz_2021-eng(7).pdf

Bajni, G., Camera, C. A., & Apuani, T. (2023). A novel dynamic rockfall susceptibility model including precipitation, temperature and snowmelt predictors: A case study in Aosta Valley (northern Italy). *Landslides*, 1–24.

Bogaard, T. A., & Greco, R. (2016). Landslide hydrology: From hydrology to pore pressure. *WIREs Water*, *3*(3), 439–459. https://doi.org/10.1002/wat2.1126

Bolker, B. M., Brooks, M. E., Clark, C. J., Geange, S. W., Poulsen, J. R., Stevens, M. H. H., & White, J. S. S. (2009). Generalized linear mixed models: A practical guide for ecology and evolution. *Trends in Ecology & Evolution*, *24*(3), 127–135. https://doi.org/10.1016/J.TREE.2008.10.008

Bornaetxea, T., Rossi, M., Marchesini, I., & Alvioli, M. (2018). Effective surveyed area and its role in statistical landslide susceptibility assessments. *Natural Hazards and Earth System Sciences*, *18*(9), 2455–2469.

Brenning, A. (2012). Spatial cross-validation and bootstrap for the assessment of prediction rules in remote sensing: The R package sperrorest. *2012 IEEE International Geoscience and Remote Sensing Symposium*, 5372–5375.

Brenning, A., Schratz, P., & Herrmann, T. (2022). *sperrorest: Perform Spatial Error Estimation and Variable Importance Assessment* (Version 3.0.5) [Computer software]. https://cran.r-project.org/web/packages/sperrorest/index.html

Brunetti, M. T., Peruccacci, S., Rossi, M., Luciani, S., Valigi, D., & Guzzetti, F. (2010). Rainfall thresholds for the possible occurrence of landslides in Italy. *Natural Hazards and Earth System Sciences*, *10*(3), 447–458.

Bryce, E., Castro-Camilo, D., Dashwood, C., Tanyas, H., Ciurean, R., Novellino, A., & Lombardo, L. (2024). An updated landslide susceptibility model and a log-Gaussian Cox process extension for Scotland. *Landslides*. https://doi.org/10.1007/s10346-024-02368-9

Budimir, M. E. A., Atkinson, P. M., & Lewis, H. G. (2015). A systematic review of landslide probability mapping using logistic regression. *Landslides*, *12*, 419–436.

Caleca, F., Confuorto, P., Raspini, F., Segoni, S., Tofani, V., Casagli, N., & Moretti, S. (2024). Shifting from traditional landslide occurrence modeling to scenario estimation with a

"glass-box" machine learning. *Science of The Total Environment*, *950*, 175277. https://doi.org/10.1016/j.scitotenv.2024.175277
Camera, C. A. S., Bajni, G., Corno, I., Raffa, M., Stevenazzi, S., & Apuani, T. (2021). Introducing intense rainfall and snowmelt variables to implement a process-related non-stationary shallow landslide susceptibility analysis. *Science of the Total Environment*, *786*. https://doi.org/10.1016/J.SCITOTENV.2021.147360
Conrad, O., Bechtel, B., Bock, M., Dietrich, H., Fischer, E., Gerlitz, L., Wehberg, J., Wichmann, V., & Böhner, J. (2015). System for Automated Geoscientific Analyses (SAGA) v. 2.1.4. *Geoscientific Model Development*, *8*(7), 1991–2007. https://doi.org/10.5194/gmd-8-1991-2015
Corominas, J., Westen, C. van, Frattini, P., Cascini, L., Malet, J. P., Fotopoulou, S., Catani, F., Eeckhaut, M. V. D., Mavrouli, O., Agliardi, F., Pitilakis, K., Winter, M. G., Pastor, M., Ferlisi, S., Tofani, V., Herv\a'as, J., & Smith, J. T. (2014). Recommendations for the quantitative analysis of landslide risk. *Bulletin of Engineering Geology and the Environment*, *73*(2), 209–263. https://doi.org/10.1007/S10064-013-0538-8/FIGURES/5
Crespi, A., Matiu, M., Bertoldi, G., Petitta, M., & Zebisch, M. (2021). A high-resolution gridded dataset of daily temperature and precipitation records (1980-2018) for Trentino-South Tyrol (north-eastern Italian Alps). *Earth System Science Data*, *13*(6), 2801–2818. https://doi.org/10.5194/ESSD-13-2801-2021
Crozier, M. J. (1986). *Landslides: Causes, Consequences & Environment*. Croom Helm. https://books.google.it/books?id=0Rs-AAAAIAAJ
Dahal, A., Tanyaş, H., & Lombardo, L. (2024). Full seismic waveform analysis combined with transformer neural networks improves coseismic landslide prediction. *Communications Earth & Environment*, *5*(1), 1–11. https://doi.org/10.1038/s43247-024-01243-8
Dahal, A., Tanyas, H., van Westen, C., van der Meijde, M., Mai, P. M., Huser, R., & Lombardo, L. (2024). Space–time landslide hazard modeling via Ensemble Neural Networks. *Natural Hazards and Earth System Sciences*, *24*(3), 823–845. https://doi.org/10.5194/nhess-24-823-2024
de Vugt, L., Zieher, T., Schneider-Muntau, B., Moreno, M., Steger, S., & Rutzinger, M. (2024). Spatial transferability of the physically based model TRIGRS using parameter ensembles. *Earth Surface Processes and Landforms*. https://doi.org/10.1002/esp.5770
Dietrich, H., & Böhner, J. (2008). Cold air production and flow in a low mountain range landscape in Hessia (Germany). *Hamburger Beiträge Zur Physischen Geographie Und Landschaftsökologie*, *19*, 37–48.
Elia, L., Castellaro, S., Dahal, A., & Lombardo, L. (2023). Assessing multi-hazard susceptibility to cryospheric hazards: Lesson learnt from an Alaskan example. *Science of The Total Environment*, *898*, 165289. https://doi.org/10.1016/j.scitotenv.2023.165289
Fang, Z., Tanyas, H., Gorum, T., Dahal, A., Wang, Y., & Lombardo, L. (2023). Speech-recognition in landslide predictive modelling: A case for a next generation early warning system. *Environmental Modelling & Software*, *170*, 105833. https://doi.org/10.1016/j.envsoft.2023.105833
Fell, R., Corominas, J., Bonnard, C., Cascini, L., Leroi, E., & Savage, W. Z. (2008). Guidelines for landslide susceptibility, hazard and risk zoning for land use planning. *Engineering Geology*, *102*(3–4), 83–84. https://doi.org/10.1016/J.ENGGEO.2008.03.009

Froude, M. J., & Petley, D. N. (2018). Global fatal landslide occurrence from 2004 to 2016. *Natural Hazards and Earth System Sciences*, *18*(8), 2161–2181. https://doi.org/10.5194/nhess-18-2161-2018

Gariano, S. L., Brunetti, M. T., Iovine, G., Melillo, M., Peruccacci, S., Terranova, O., Vennari, C., & Guzzetti, F. (2015). Calibration and validation of rainfall thresholds for shallow landslide forecasting in Sicily, southern Italy. *Geomorphology*, *228*, 653–665.

Gariano, S. L., & Guzzetti, F. (2016). Landslides in a changing climate. *Earth-Science Reviews*, *162*, 227–252. https://doi.org/10.1016/J.EARSCIREV.2016.08.011

Geokatalog. (2019). *Open Geodatabase of the Autonomous Province of South Tyrol*. https://geoportal.buergernetz.bz.it/geodaten.asp

Ghaemi, E., Foelsche, U., Kann, A., & Fuchsberger, J. (2021). Evaluation of Integrated Nowcasting through Comprehensive Analysis (INCA) precipitation analysis using a dense rain-gauge network in southeastern Austria. *Hydrol. Earth Syst. Sci*, *25*, 4335–4356. https://doi.org/10.5194/hess-25-4335-2021

Glade, T., Anderson, M., & Crozier, M. J. (2012). Landslide Hazard and Risk. In *Landslide Hazard and Risk*. Wiley Blackwell. https://doi.org/10.1002/9780470012659

Goetz, J., Brenning, A., Marcer, M., & Bodin, X. (2018). Modeling the precision of structure-from-motion multi-view stereo digital elevation models from repeated close-range aerial surveys. *Remote Sensing of Environment*, *210*, 208–216. https://doi.org/10.1016/j.rse.2018.03.013

Goetz, J., Brenning, A., Petschko, H., & Leopold, P. (2015). Evaluating machine learning and statistical prediction techniques for landslide susceptibility modeling. *Computers & Geosciences*, *81*, 1–11. https://doi.org/10.1016/j.cageo.2015.04.007

Goldsmith, J., Scheipl, F., Huang, L., Wrobel, J., Di, C., Gellar, J., Harezlak, J., McLean, M. W., Swihart, B., Xiao, L., Crainiceanu, C., Reiss, P. T., Chen, Y., Greven, S., Huo, L., Kundu, M. G., Park, S. Y., Miller, D. L., Staicu, A.-M., … Li, Z. (2024). *refund: Regression with Functional Data* (Version 0.1-35) [Computer software]. https://cran.r-project.org/web/packages/refund/index.html

Gómez, D., Aristizábal, E., García, E. F., Marín, D., Valencia, S., & Vásquez, M. (2023). Landslides forecasting using satellite rainfall estimations and machine learning in the Colombian Andean region. *Journal of South American Earth Sciences*, *125*, 104293. https://doi.org/10.1016/j.jsames.2023.104293

Greco, R., Marino, P., & Bogaard, T. A. (2023). Recent advancements of landslide hydrology. *WIREs Water*, *10*(6), e1675. https://doi.org/10.1002/wat2.1675

Guzzetti, F., Gariano, S. L., Peruccacci, S., Brunetti, M. T., Marchesini, I., Rossi, M., & Melillo, M. (2020). Geographical landslide early warning systems. *Earth-Science Reviews*, *200*, 102973. https://doi.org/10.1016/J.EARSCIREV.2019.102973

Guzzetti, F., Reichenbach, P., Cardinali, M., Galli, M., & Ardizzone, F. (2005). Probabilistic landslide hazard assessment at the basin scale. *Geomorphology*, *72*(1–4), 272–299.

Haiden, T., Kann, A., Wittmann, C., Pistotnik, G., Bica, B., & Gruber, C. (2011). The Integrated Nowcasting through Comprehensive Analysis (INCA) System and Its Validation over the Eastern Alpine Region. *Weather and Forecasting*, *26*(2), 166–183. https://doi.org/10.1175/2010WAF2222451.1

Hosmer, D. W., Lemeshow, S., & Sturdivant, R. X. (2013). Applied Logistic Regression: Third Edition. *Applied Logistic Regression: Third Edition*, 1–510. https://doi.org/10.1002/9781118548387

Iadanza, C., Trigila, A., Starace, P., Dragoni, A., Biondo, T., & Roccisano, M. (2021). IdroGEO: A Collaborative Web Mapping Application Based on REST API Services and Open Data on Landslides and Floods in Italy. *ISPRS International Journal of Geo-Information*, *10*(2), Article 2. https://doi.org/10.3390/ijgi10020089

IPCC, B. (Ed.). (2022). *Climate Change 2022: Impacts, Adaptation and Vulnerability. Contribution of Working Group II to the Sixth Assessment Report of the Intergovernmental Panel on Climate Change.*

Jakob, M. (2022). Chapter 14—Landslides in a changing climate. In T. Davies, N. Rosser, & J. F. Shroder (Eds.), *Landslide Hazards, Risks, and Disasters (Second Edition)* (pp. 505–579). Elsevier. https://doi.org/10.1016/B978-0-12-818464-6.00003-2

Kirschbaum, D., Stanley, T., & Zhou, Y. (2015). Spatial and temporal analysis of a global landslide catalog. *Geomorphology*, *249*, 4–15. https://doi.org/10.1016/J.GEOMORPH.2015.03.016

Knevels, R., Petschko, H., Proske, H., Leopold, P., Maraun, D., & Brenning, A. (2020). Event-based landslide modeling in the Styrian basin, Austria: Accounting for time-varying rainfall and land cover. *Geosciences 2020, Vol. 10, Page 217*, *10*(6), 217. https://doi.org/10.3390/GEOSCIENCES10060217

Lim, J., Santinelli, G., Dahal, A., Vrieling, A., & Lombardo, L. (2024). An ensemble neural network approach for space–time landslide predictive modelling. *International Journal of Applied Earth Observation and Geoinformation*, *132*, 104037. https://doi.org/10.1016/j.jag.2024.104037

Lima, P., Steger, S., & Glade, T. (2021). Counteracting flawed landslide data in statistically based landslide susceptibility modelling for very large areas: A national-scale assessment for Austria. *Landslides*, *18*(11), 3531–3546.

Lin, Q., Lima, P., Steger, S., Glade, T., Jiang, T., Zhang, J., Liu, T., & Wang, Y. (2021). National-scale data-driven rainfall induced landslide susceptibility mapping for China by accounting for incomplete landslide data. *Geoscience Frontiers*, *12*(6), 101248. https://doi.org/10.1016/J.GSF.2021.101248

Loche, M., Scaringi, G., Yunus, A. P., Catani, F., Tanyaş, H., Frodella, W., Fan, X., & Lombardo, L. (2022). Surface temperature controls the pattern of post-earthquake landslide activity. *Scientific Reports*, *12*(1), 988. https://doi.org/10.1038/s41598-022-04992-8

Lombardo, L., Opitz, T., Ardizzone, F., Guzzetti, F., & Huser, R. (2020). Space-time landslide predictive modelling. *Earth-Science Reviews*, *209*, 103318.

Maraun, D., Knevels, R., Mishra, A. N., Truhetz, H., Bevacqua, E., Proske, H., Zappa, G., Brenning, A., Petschko, H., Schaffer, A., Leopold, P., & Puxley, B. L. (2022). A severe landslide event in the Alpine foreland under possible future climate and land-use changes. *Communications Earth & Environment*, *3*(1), 1–11. https://doi.org/10.1038/s43247-022-00408-7

Marra, F., Nikolopoulos, E. I., Creutin, J. D., & Borga, M. (2014). Radar rainfall estimation for the identification of debris-flow occurrence thresholds. *Journal of Hydrology*, *519*(PB), 1607–1619. https://doi.org/10.1016/J.JHYDROL.2014.09.039

Marra, F., Nikolopoulos, E. I., Creutin, J. D., & Borga, M. (2016). Space–time organization of debris flows-triggering rainfall and its effect on the identification of the rainfall threshold relationship. *Journal of Hydrology*, *541*, 246–255. https://doi.org/10.1016/j.jhydrol.2015.10.010

McLean, M. W., Hooker, G., Staicu, A.-M., Scheipl, F., & Ruppert, D. (2014). Functional Generalized Additive Models. *Journal of Computational and Graphical Statistics : A Joint Publication of American Statistical Association, Institute of Mathematical Statistics, Interface Foundation of North America*, *23*(1), 249–269. https://doi.org/10.1080/10618600.2012.729985

Monsieurs, E., Dewitte, O., Depicker, A., & Demoulin, A. (2019). Towards a transferable antecedent rainfall—Susceptibility threshold approach for landsliding. *Water*, *11*(11), Article 11. https://doi.org/10.3390/w11112202

Moreno, M., Lombardo, L., Crespi, A., Zellner, P. J., Mair, V., Pittore, M., van Westen, C., & Steger, S. (2024). Space-time data-driven modeling of precipitation-induced shallow landslides in South Tyrol, Italy. *Science of The Total Environment*, *912*, 169166. https://doi.org/10.1016/j.scitotenv.2023.169166

Moreno, M., Steger, S., Tanyas, H., & Lombardo, L. (2023). Modeling the area of co-seismic landslides via data-driven models: The Kaikōura example. *Engineering Geology*, *320*, 107121.

Morris, J. S. (2015). Functional Regression. *Annual Review of Statistics and Its Application*, *2*(1), 321–359. https://doi.org/10.1146/annurev-statistics-010814-020413

Nadim, F., Kjekstad, O., Peduzzi, P., Herold, C., & Jaedicke, C. (2006, May). Global landslide and avalanche hotspots. In *Landslides* (Vol. 3, Issue 2, pp. 159–173). Springer. https://doi.org/10.1007/s10346-006-0036-1

Niyokwiringirwa, P., Lombardo, L., Dewitte, O., Deijns, A. A. J., Wang, N., Van Westen, C. J., & Tanyas, H. (2024). Event-based rainfall-induced landslide inventories and rainfall thresholds for Malawi. *Landslides*, *21*(6), 1403–1424. https://doi.org/10.1007/s10346-023-02203-7

Nocentini, N., Rosi, A., Segoni, S., & Fanti, R. (2023). Towards landslide space-time forecasting through machine learning: The influence of rainfall parameters and model setting. *Frontiers in Earth Science*, *11*. https://doi.org/10.3389/feart.2023.1152130

Opitz, T., Bakka, H., Huser, R., & Lombardo, L. (2022). High-resolution Bayesian mapping of landslide hazard with unobserved trigger event. *The Annals of Applied Statistics*, *16*(3), 1653–1675. https://doi.org/10.1214/21-AOAS1561

Ozturk, U., Bozzolan, E., Holcombe, E. A., Shukla, R., Pianosi, F., & Wagener, T. (2022). How climate change and unplanned urban sprawl bring more landslides. *Nature*, *608*(7922), 262–265. https://doi.org/10.1038/d41586-022-02141-9

Pedersen, E. J., Miller, D. L., Simpson, G. L., & Ross, N. (2019). Hierarchical generalized additive models in ecology: An introduction with mgcv. *PeerJ*, *2019*(5), e6876. https://doi.org/10.7717/PEERJ.6876/SUPP-1

Peruccacci, S., Brunetti, M. T., Gariano, S. L., Melillo, M., Rossi, M., & Guzzetti, F. (2017). Rainfall thresholds for possible landslide occurrence in Italy. *Geomorphology*, *290*, 39–57.

Piacentini, D., Troiani, F., Soldati, M., Notarnicola, C., Savelli, D., Schneiderbauer, S., & Strada, C. (2012). Statistical analysis for assessing shallow-landslide susceptibility in South Tyrol (south-eastern Alps, Italy). *Geomorphology*, *151–152*, 196–206. https://doi.org/10.1016/J.GEOMORPH.2012.02.003

Ramsay, J. O., & Silverman, B. W. (2005). *Functional Data Analysis*. Springer. https://doi.org/10.1007/b98888

Reichenbach, P., Rossi, M., Malamud, B. D., Mihir, M., & Guzzetti, F. (2018, May). A review of statistically-based landslide susceptibility models. In *Earth-Science Reviews* (Vol. 180, pp. 60–91). Elsevier B.V. https://doi.org/10.1016/j.earscirev.2018.03.001

Schlögel, R., Kofler, C., Gariano, S. L., Campenhout, J. V., & Plummer, S. (2020). Changes in climate patterns and their association to natural hazard distribution in South Tyrol (Eastern Italian Alps). *Scientific Reports 2020 10:1*, *10*(1), 1–14. https://doi.org/10.1038/s41598-020-61615-w

Segoni, S., Piciullo, L., & Gariano, S. L. (2018). A review of the recent literature on rainfall thresholds for landslide occurrence. *Landslides*, *15*(8), 1483–1501. https://doi.org/10.1007/S10346-018-0966-4/FIGURES/2

Smith, H. G., Neverman, A. J., Betts, H., & Spiekermann, R. (2023). The influence of spatial patterns in rainfall on shallow landslides. *Geomorphology*, *437*, 108795. https://doi.org/10.1016/j.geomorph.2023.108795

Stanley, T. A., Kirschbaum, D. B., Benz, G., Emberson, R. A., Amatya, P. M., Medwedeff, W., & Clark, M. K. (2021). Data-Driven landslide nowcasting at the global scale. *Frontiers in Earth Science*, *9*, 378. https://doi.org/10.3389/FEART.2021.640043/BIBTEX

Steger, S., Brenning, A., Bell, R., & Glade, T. (2017). The influence of systematically incomplete shallow landslide inventories on statistical susceptibility models and suggestions for improvements. *Landslides*, *14*(5), 1767–1781.

Steger, S., & Glade, T. (2017). The challenge of "trivial areas" in statistical landslide susceptibility modelling. In M. Mikos, B. Tiwari, Y. Yin, & K. Sassa (Eds.), *Advancing Culture of Living with Landslides* (pp. 803–808). Springer International Publishing.

Steger, S., Mair, V., Kofler, C., Pittore, M., Zebisch, M., & Schneiderbauer, S. (2021). Correlation does not imply geomorphic causation in data-driven landslide susceptibility modelling – Benefits of exploring landslide data collection effects. *Science of The Total Environment*, *776*, 145935. https://doi.org/10.1016/j.scitotenv.2021.145935

Steger, S., Moreno, M., Crespi, A., Luigi Gariano, S., Teresa Brunetti, M., Melillo, M., Peruccacci, S., Marra, F., de Vugt, L., Zieher, T., Rutzinger, M., Mair, V., & Pittore, M. (2024). Adopting the margin of stability for space–time landslide prediction – A data-driven approach for generating spatial dynamic thresholds. *Geoscience Frontiers*, *15*(5), 101822. https://doi.org/10.1016/j.gsf.2024.101822

Steger, S., Moreno, M., Crespi, A., Zellner, P. J., Gariano, S. L., Brunetti, M. T., Melillo, M., Peruccacci, S., Marra, F., Kohrs, R., & others. (2023). Deciphering seasonal effects of triggering and preparatory precipitation for improved shallow landslide prediction<? Xmltex\backslashbreak?> using generalized additive mixed models. *Natural Hazards and Earth System Sciences*, *23*(4), 1483–1506.

Stingl, V., & Mair, V. (2005). *Introduzione alla geologia dell'Alto Adige*. Provincia Autonoma di Bolzano-Alto-Adige. https://books.google.it/books?id=ei5jMwEACAAJ

Tanyas, H., Rossi, M., Alvioli, M., van Westen, C. J., & Marchesini, I. (2019). A global slope unit-based method for the near real-time prediction of earthquake-induced landslides. *Geomorphology*, *327*, 126–146. https://doi.org/10.1016/j.geomorph.2018.10.022

Tasser, E., Mader, M., & Tappeiner, U. (2003). Effects of land use in alpine grasslands on the probability of landslides. *Basic and Applied Ecology*, *4*(3), 271–280.

Thomas, M. A., Collins, B. D., & Mirus, B. B. (2019). Assessing the Feasibility of Satellite-Based Thresholds for Hydrologically Driven Landsliding. *Water Resources Research*, *55*(11), 9006–9023. https://doi.org/10.1029/2019WR025577

Trigila, A., Iadanza, C., & Spizzichino, D. (2010). Quality assessment of the Italian Landslide Inventory using GIS processing. *Landslides*, *7*(4), 455–470.

Wang, N., Cheng, W., Marconcini, M., Bachofer, F., Liu, C., Xiong, J., & Lombardo, L. (2022). Space-time susceptibility modeling of hydro-morphological processes at the Chinese national scale. *Engineering Geology*, *301*, 106586. https://doi.org/10.1016/J.ENGGEO.2022.106586

Westen, C. J. van, Asch, T. W. J. van, & Soeters, R. (2006). Landslide hazard and risk zonation—Why is it still so difficult? *Bulletin of Engineering Geology and the Environment*, *65*(2), 167–184. https://doi.org/10.1007/S10064-005-0023-0/FIGURES/5

Westen, C. J. van, Castellanos, E., & Kuriakose, S. L. (2008). Spatial data for landslide susceptibility, hazard, and vulnerability assessment: An overview. *Engineering Geology*, *102*(3–4), 112–131. https://doi.org/10.1016/J.ENGGEO.2008.03.010

Wicki, A., Lehmann, P., Hauck, C., Seneviratne, S. I., Waldner, P., & Stähli, M. (2020). Assessing the potential of soil moisture measurements for regional landslide early warning. *Landslides*, *17*(8), 1881–1896. https://doi.org/10.1007/s10346-020-01400-y

Wood, S. N. (2017). *Generalized Additive Models: An Introduction with R, Second Edition* (2nd ed.). Chapman and Hall/CRC. https://doi.org/10.1201/9781315370279

Zuur, A. F., Ieno, E. N., Walker, N., Saveliev, A. A., & Smith, G. M. (2009). *Mixed effects models and extensions in ecology with R*. Springer New York. https://doi.org/10.1007/978-0-387-87458-6